Behavioral/Systems/Cognitive

Neuronal Basis of the Slow (<1 Hz) Oscillation in Neurons of the Nucleus Reticularis Thalami *In Vitro*

Kate L. Blethyn, Stuart W. Hughes, Tibor I. Tóth, David W. Cope, and Vincenzo Crunelli
School of Biosciences, Cardiff University, Cardiff CF10 3US, United Kingdom

During deep sleep and anesthesia, the EEG of humans and animals exhibits a distinctive slow (<1 Hz) rhythm. In inhibitory neurons of the nucleus reticularis thalami (NRT), this rhythm is reflected as a slow (<1 Hz) oscillation of the membrane potential comprising stereotypical, recurring "up" and "down" states. Here we show that reducing the leak current through the activation of group I metabotropic glutamate receptors (mGluRs) with either *trans*-ACPD [(+/−)-1-aminocyclopentane-*trans*-1,3-dicarboxylic acid] (50–100 μM) or DHPG [(*S*)-3,5-dihydroxyphenylglycine] (100 μM) instates an intrinsic slow oscillation in NRT neurons *in vitro* that is qualitatively equivalent to that observed *in vivo*. A slow oscillation could also be evoked by synaptically activating mGluRs on NRT neurons via the tetanic stimulation of corticothalamic fibers. Through a combination of experiments and computational modeling we show that the up state of the slow oscillation is predominantly generated by the "window" component of the T-type Ca^{2+} current, with an additional supportive role for a Ca^{2+}-activated nonselective cation current. The slow oscillation is also fundamentally reliant on an I_h current and is extensively shaped by both Ca^{2+}- and Na^+-activated K^+ currents. In combination with previous work in thalamocortical neurons, this study suggests that the thalamus plays an important and active role in shaping the slow (<1 Hz) rhythm during deep sleep.

Key words: **sleep; EEG; rhythm; thalamus; calcium current; T-type; mGluR; CAN current**

Introduction

During deep sleep and under certain types of anesthesia, the EEG of humans and animals is characterized by the slow (<1 Hz) rhythm (Steriade et al., 1993a,b; Simon et al., 2000, 2003). In cortical neurons, this rhythm is correlated with alternating episodes of intense synaptic barrages and disfacilitation leading to distinct "up" and "down" membrane potential states (Steriade et al., 1993a, 2001; Contreras and Steriade, 1995; Sanchez-Vives and McCormick, 2000). In the thalamus, the cellular counterpart of the slow rhythm in both glutamatergic thalamocortical (TC) neurons and GABAergic neurons of the nucleus reticularis thalami (NRT) is also characterized by recurring up and down states (Steriade et al., 1993c; Contreras and Steriade, 1995; Timofeev and Steriade, 1996). However, in these cell types, up and down states appear to be formed more by a stereotypical slow (<1 Hz) oscillation than simple variations in synaptic activity (Contreras and Steriade, 1995; Crunelli et al., 2002). Consistent with this, we recently showed that after activation of the metabotropic glutamate receptor (mGluR) that is postsynaptic to cortical input, mGluR1a, TC neurons *in vitro* exhibit an intrinsic slow oscillation with identical properties to those observed *in vivo* (Hughes et al., 2002a). This result therefore challenged the notion that the slow rhythm *in vivo* is exclusively generated by cortical network operations (Steriade et al., 1993b; Sanchez-Vives and McCormick, 2000).

In TC neurons, the intrinsic slow oscillation arises when mGluR1a activation reduces the leak K^+ current, I_{Leak}, below a certain threshold where it can interact with the "window" component of the T-type Ca^{2+} current, $I_{Twindow}$, to produce a form of intrinsic bistability (Williams et al., 1997; Tóth et al., 1998; Hughes et al., 1999, 2002a). The slow oscillation in TC neurons also relies on a Ca^{2+}-activated, nonselective cation (CAN) current (Hughes et al., 2002a; Crunelli et al., 2005). Because neurons in the NRT (1) exhibit a substantial I_T window current (Huguenard and Prince, 1992; Klockner et al., 1999; Talley et al., 1999; Perez-Reyes, 2003), (2) are subject to a reduction in I_{Leak} after mGluR activation (Lee and McCormick, 1997; Cox and Sherman, 1999), and (3) possess a prominent CAN current (Bal and McCormick, 1993), we recently predicted that activation of mGluRs could also bring about an intrinsic slow oscillation in this cell type (Crunelli et al., 2005).

In this study, we confirm that mGluR activation is a reliable pathway for inducing an intrinsic slow oscillation in NRT neurons *in vitro* with properties that are qualitatively equivalent to those observed *in vivo* (Steriade et al., 1986, 1993c; Contreras and Steriade, 1995; Timofeev and Steriade, 1996). We also show that this oscillation requires the specific stimulation of mGluR1a and that it depends primarily on $I_{Twindow}$. This activity also involves a number of additional intrinsic conductances, which combine to shape its unique properties. This study, therefore, further endorses the idea that the thalamus actively influences the slow (<1 Hz) rhythm in the whole brain.

Received Aug. 25, 2005; revised Jan. 13, 2006; accepted Jan. 16, 2006.

This work was supported by Wellcome Trust Grant 71436. Additional information regarding this and other published work from the Crunelli laboratory is available at http://www.thalamus.org.uk. We thank T. M. Gould for technical assistance.

Correspondence should be addressed to S. W. Hughes, School of Biosciences, Cardiff University, Museum Avenue, Cardiff CF10 3US, UK. E-mail: HughesSW@Cardiff.ac.uk.

DOI:10.1523/JNEUROSCI.3607-05.2006

 0270-6474/06/262474-13$15.00/0

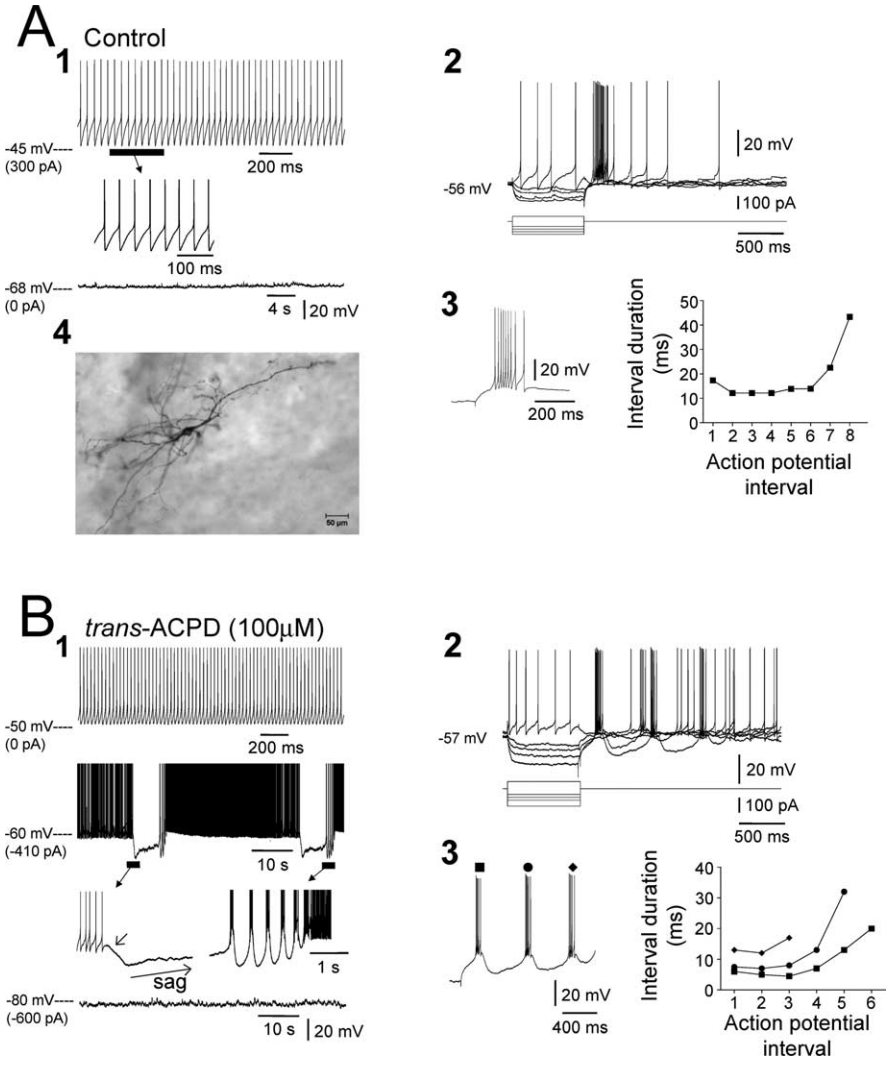

Figure 1. *Trans*-ACPD instates a slow (<1 Hz) oscillation in NRT neurons. ***A*$_1$**, Intracellular recording of an NRT neuron in the PGN exhibiting a quiescent resting membrane potential in the absence of DC current (bottom trace) and continuous tonic firing in response to steady depolarizing current (300 pA; top trace). ***A*$_2$**, Response of the neuron to brief hyperpolarizing and depolarizing current steps. Note the presence of an LTCP-mediated burst at the offset of the voltage response to a sufficiently large hyperpolarizing current pulse (enlarged in ***A*$_3$**). This burst displays a characteristic accelerating–decelerating pattern of action potential output (Domich et al., 1986) (***A*$_3$**, right plot). ***A*$_4$**, Morphological reconstruction of the neuron from which the traces in ***A*$_1$**–***A*$_3$** were obtained. Note the characteristic elongated soma and bipolar dendritic field (Uhlrich et al., 1991). ***B*$_1$**, Application of *trans*-ACPD (100 μM) depolarized the NRT neuron such that in the absence of DC current, spontaneous tonic action potential firing was apparent (top trace). Injection of hyperpolarizing DC current (−410 pA) revealed the presence of a slow (<1 Hz) membrane potential oscillation. Note the presence of the slow depolarizing sag during the down state and intense action potential firing during the up state. Enlargements of the transitions from up to down state and down to up state reveal the presence of a membrane potential inflection (see arrow in left enlargement) and a group of LTCP bursts (right enlargement), respectively. Injection of additional hyperpolarizing DC current abolished the slow oscillation, leading to a quiescent hyperpolarized membrane potential (bottom trace). ***B*$_2$**, *trans*-ACPD causes a clear increase in apparent input resistance (R_N). In addition, *trans*-ACPD enhanced the ability of the neuron to exhibit rebound bursting such that at the offset of voltage responses to sufficiently large hyperpolarizing current pulses, this neuron became able to exhibit rhythmic groups of LTCP bursts rather than just a single burst (enlarged in ***B*$_3$**). Again, note the characteristic accelerating–decelerating pattern of action potential output of these bursts (***B*$_3$**, right plot). Action potentials have been truncated in this figure.

Materials and Methods

Experiments were performed in accordance with local ethical committee guidelines and the United Kingdom Animals (Scientific Procedure) Act, 1986. All efforts were made to minimize the suffering and number of animals used in each experiment.

In vitro *slice preparation and maintenance*. Young adult cats (1–1.5 kg) were deeply anesthetized with a mixture of O_2 and NO_2 (2:1) and 2.5% halothane, wide craniotomies were performed, and the brains removed. Sagittal slices (450–500 μm) of the thalamus containing either the lateral geniculate nucleus (LGN), ventrolateral (VL) nucleus, or ventrobasal (VB) nuclei and the associated sectors of the NRT [i.e., perigeniculate nucleus (PGN), peri-VL sector, or peri-VB sector, respectively] were prepared and maintained as described previously (Hughes et al., 2002a). For recording, slices were perfused with a warmed (35 ± 1°C), continuously oxygenated (95% O_2, 5% CO_2) artificial CSF (ACSF) containing the following (in mM): 134 NaCl, 2 KCl, 1.25 KH_2PO_4, 1 $MgSO_4$, 2 $CaCl_2$, 16 $NaHCO_3$, 10 glucose. For experiments involving $NiCl_2$ or $CdCl_2$, $MgSO_4$ was replaced with $MgCl_2$ and KH_2PO_4 was omitted. All drugs were dissolved directly in ACSF. Drugs were obtained from the following sources: DL-2-amino-5-phosphonovaleric acid (DL-AP5) (NMDA receptor antagonist), (+)-2-methyl-4-carboxyphenylglycine (LY367385) (mGluR1a selective antagonist), [*S*-(*R**,*R**)]-[3-[[1-(3,4-dichlorophenyl)ethyl]amino]-2-hydroxypropyl](cyclohexylmethyl)phosphinic acid (CGP54626) ($GABA_B$ receptor antagonist), 6-cyano-7-nitroquinoxaline-2,3-dione (CNQX) (AMPA/kainate receptor antagonist), (*S*)-3,5-dihydroxyphenylglycine (DHPG) (group I selective mGluR agonist), 6-imino-3-(4-methoxyphenyl)-1(6*H*)-pyridazinebutanoic acid hydrobromide (SR95531) ($GABA_A$ receptor antagonist), (+/−)-1-aminocyclopentane-*trans*-1,3-dicarboxylic acid (*trans*-ACPD) (nonselective group I/II mGluR agonist), tetrodotoxin (TTX) (Na^+ channel blocker), and 4-(*N*-ethyl-*N*-phenylamino)-1,2-dimethyl-6-(methylamino)-pyrimidinium chloride (ZD7288) (h-channel blocker) from Tocris Cookson (Bristol, UK); apamin [small conductance $I_{K(Ca)}$ (SK) channel blocker] from Sigma (Poole, UK).

In vitro *electrophysiology*. Extracellular single-unit recordings were performed using glass pipettes filled with 0.5 M NaCl (resistance, 1–5 MΩ) connected to a Neurolog 104 differential amplifier (Digitimer, Welwyn Garden City, UK), with the resulting signal being filtered at 0.2–20 kHz. Intracellular recordings, using the current-clamp technique, were performed with standard or thin wall glass microelectrodes filled with 1 M potassium acetate (resistance, 80–120 MΩ or 30–60 MΩ, respectively), and in some cases 2% biocytin, and connected to an Axoclamp-2A amplifier (Molecular Devices, Foster City, CA) operating in bridge mode. Impaled cells were identified as NRT neurons using established electrophysiological and morphological criteria (Uhlrich et al., 1991; Bal and McCormick, 1993; Contreras et al., 1993). The apparent input resistance (R_N) was estimated from voltage responses evoked at −60 mV by small (20–50 pA) hyperpolarizing current steps. Only neurons with overshooting action potentials and an R_N>50 MΩ were selected for further experimentation and analysis. In slices where neurons had been filled with biocytin, visualization of the dye was performed as described previously (Hughes et al., 2002b). Voltage and current records were stored on a Biologic DAT recorder (IntraCel, Royston, UK) and later analyzed using Clampfit (Molecular Devices). The effect of apamin on extracellular recordings was assessed after the slices had been exposed to this drug for at least 30 min. In all experiments, statistical significance was assessed using Student's *t* test.

Stimulation of corticothalamic fibers was performed in sagittal slices

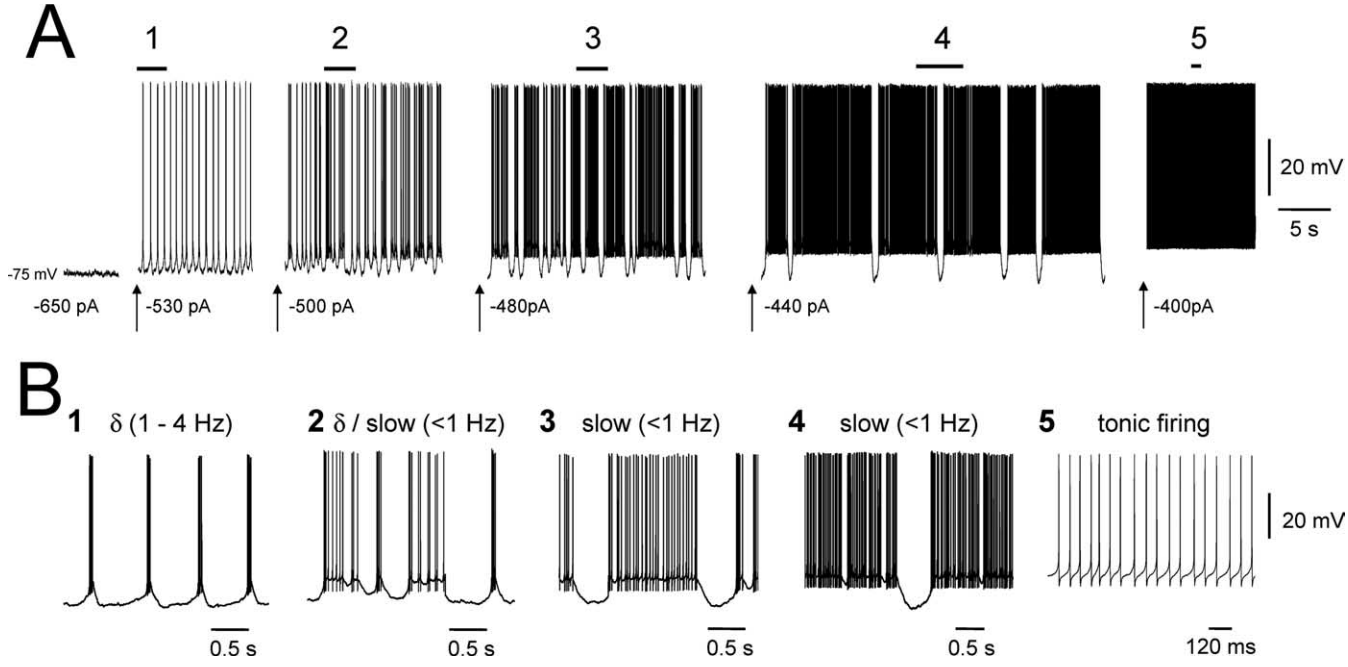

Figure 2. The slow (<1 Hz) oscillation forms part of a continuum of activity in NRT neurons. ***A***, Intracellular recording of an NRT neuron in the PGN in the presence of *trans*-ACPD (100 μM) displaying a continuum of oscillatory activity at different levels of DC current. Sections marked above are expanded in ***B***. Injection of sufficient hyperpolarizing DC current abolished all oscillatory activity (−650 pA). As this negative DC current was gradually removed, a diverse range of oscillatory activity became evident. Initially, rhythmic LTCP bursts at δ frequencies (1–4 Hz) occurred (−530 pA), later δ (1–4 Hz) and slow (<1 Hz) oscillatory activity were apparent together (−500 pA). As the negative DC current was further removed, a slow oscillation was present in isolation (−480 pA, −440 pA). Removal of further DC current abolished the slow oscillation and led to continuous tonic firing (−400 pA). ***B***, Expanded sections as indicated in ***A***. CNQX (10 μM), APV (50 μM), SR95531 (20 μM), and CGP54626 (20 μM) were present in the recording medium for the experiment depicted in this figure.

of the LGN-PGN using a bipolar tungsten electrode placed in the optic radiation (50 Hz for 500 ms, with each stimulus being a 0.2 ms pulse of 300 μA). Thalamic stimulation was also performed in sagittal LGN-PGN slices, using identical parameters, with the bipolar electrode positioned in lamina A of the LGN. All stimulation experiments were performed in the presence of CNQX (10 μM), APV (50 μM), SR95531 (20 μM), and CGP54626 (20 μM).

Dynamic clamp and computational modeling. The dynamic clamp system was implemented as described previously (Hughes et al., 1998, 1999, 2002a). The model NRT neuron was of the single-compartment Hodgkin and Huxley (1952) type and possessed the following voltage- and intracellular ion-gated currents: a fast inactivating Na^+ current, I_{Na}; a delayed rectifier K^+ current, I_{Kdr}; a low-threshold, T-type Ca^{2+} current, I_T (Huguenard and Prince, 1992); a hyperpolarization-activated, h-type current, I_h (Brunton and Charpak, 1997); a Ca^{2+}-activated K^+ current, $I_{K(Ca)}$ (Bal and McCormick, 1993); an Na^+-activated K^+ current, $I_{K(Na)}$ (Kim and McCormick, 1998); and a Ca^{2+}-activated, nonselective cation current, I_{CAN} (Bal and McCormick, 1993; Destexhe et al., 1994). The descriptions of I_{Na} and I_{Kdr} were based on corresponding currents in TC neurons (Tóth and Crunelli, 2001). The description of I_T was constructed by adapting the experimental results of Huguenard and Prince (1992). The description of I_h was based on the experimental findings of McCormick and Pape (1990) in TC neurons with parameters modified to reflect the behavior of NRT neurons. $I_{K(Ca)}$ was modeled by using the experimental results of Huguenard and Prince (1991) and assuming a linear dependence of the conductance on the local intracellular Ca^{2+} concentration. For $I_{K(Na)}$, we adopted the model given in Dale (1993). The description of I_{CAN} was based on that constructed for TC neurons (Hughes et al., 2002a) but with modified parameter values, which take into account the differences between the two neuron types. Finally, the model also included a leak current, I_{Leak}, the conductance of which was voltage-independent. The membrane capacitance (C_m), the reversal potentials (E_{xx}), and maximal conductances (g_{xx}) of ionic currents in the model were directly estimated from experimental data using the method described in Tóth and Crunelli (2001) and are as follows: $C_m = 63.3$ pF; $E_{Kdr} = -95$ mV, $g_{Kdr} = 180$ nS; $E_{Na} = 55$ mV, $g_{Na} = 964$ nS; $E_{Ca} = 180$ mV, $g_T = 17$ nS; $E_h = -33$ mV, $g_h = 8$ nS; $E_{CAN} = 10$ mV, $g_{CAN} = 20$ nS; $E_{Leak} = -65.3$ mV, $g_{Leak} = 1.5$ nS; $g_{K(Ca)} = 3$ nS; $g_{K(Na)} = 100$ nS. The processing of the local intracellular ion concentrations was modeled according to $dc/dt = \rho I_c - \gamma(c - c_o)$, where c is the local intracellular concentration of the ions, I_C is the current carrying the ions into the cell, and ρ (9×10^{-5} nM · pA^{-1} · ms^{-1} for Ca^{2+} and 5×10^{-5} mM · pA^{-1} · ms^{-1} for Na^+), γ (5×10^{-3} ms^{-1} for Ca^{2+} and 5×10^{-4} ms^{-1} for Na^+), and c_o (1.5 nM for Ca^{2+} and 2.938 mM for Na^+) are constants. A more detailed description of the activation and inactivation properties of each ionic current in the model can be downloaded from http://www.thalamus.org.uk/downloads/nrt_model.pdf.

Results

Activation of mGluR1a instates an intrinsic slow (<1 Hz) oscillation in neurons of the NRT

In control conditions, NRT neurons recorded intracellularly exhibited either a quiescent, stable resting membrane potential (−63.4 ± 2.4 mV; $n = 50$ of 61; 82%) (Fig. 1*A*$_1$) or spontaneous tonic action potential firing at low frequencies (5.8 ± 1.7 Hz; $n = 11$ of 61; 18%). The mean R_N of these cells was 130.7 ± 13.6 MΩ ($n = 61$). All neurons exhibited electrophysiological (Fig. 1*A*$_1$–*A*$_3$) and morphological (Fig. 1*A*$_4$) characteristics consistent with previous descriptions of this cell type (Uhlrich et al., 1991; Bal and McCormick, 1993; Contreras et al., 1993). In particular, at the offset of sufficiently large hyperpolarizing current steps, 87% ($n = 53$ of 61) of NRT neurons generated one or more low-threshold Ca^{2+} potentials (LTCPs), which gave rise to bursts of action potentials that displayed a distinctive accelerating-decelerating pattern (Fig. 1*A*$_2$,*A*$_3$) (Domich et al., 1986). In addition, these LTCPs were often ensued by a transient period of rhythmic single-spike activity (Domich et al., 1986; Bal and McCormick, 1993; Brunton and Charpak, 1997). Application of the nonspecific group I/II mGluR agonist *trans*-ACPD (100 μM) caused a depolarization of NRT neurons such that, in the absence

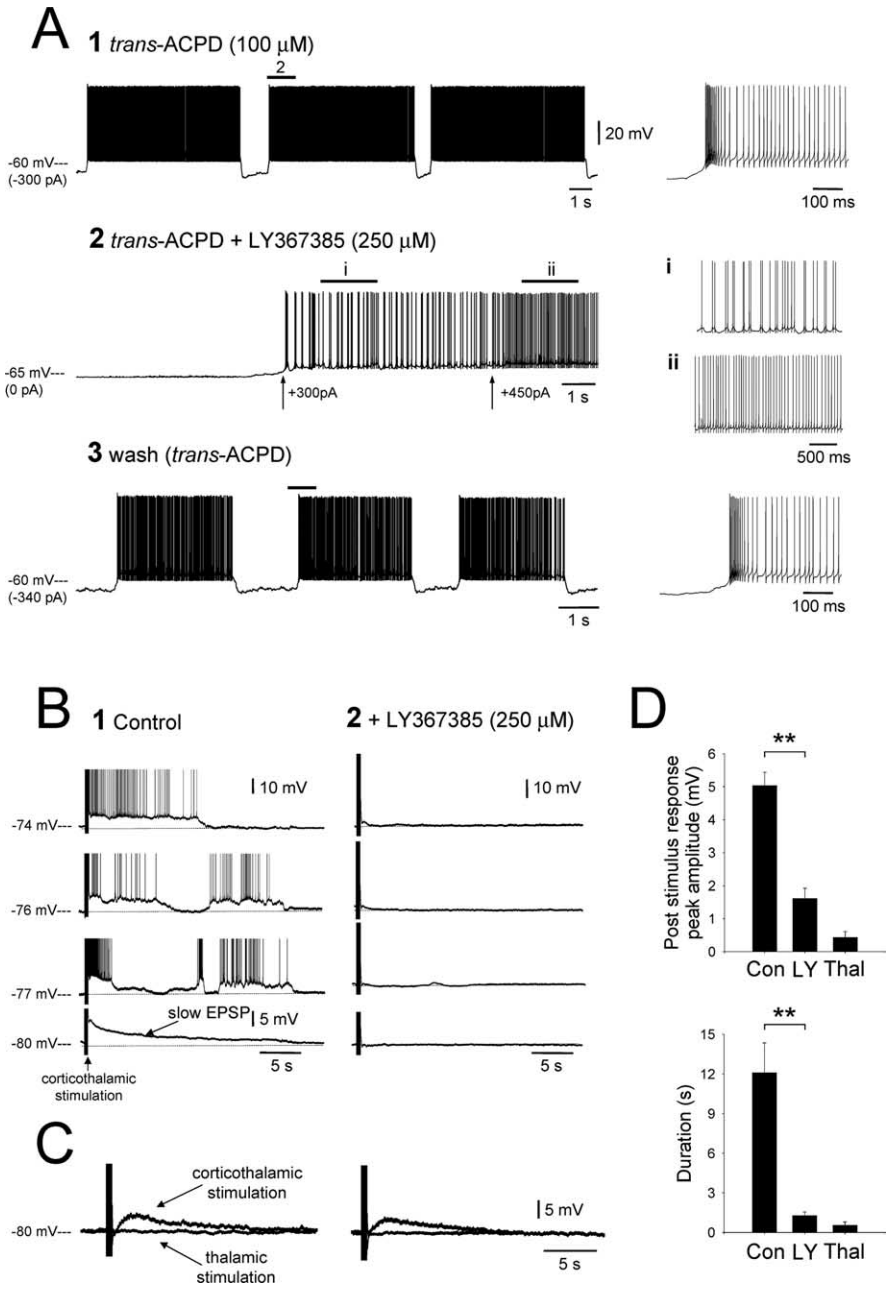

Figure 3. The capacity to generate a slow (<1 Hz) oscillation is blocked by the selective mGluR1a antagonist LY367385. ***A***, Intracellular recording of an NRT neuron in the peri-VB sector exhibiting a slow oscillation in the presence of *trans*-ACPD (100 μM) (***A*$_1$**). Addition of LY367385 (250 μM) hyperpolarizes the neuron and blocks its ability to generate slow oscillatory activity (***A*$_2$**). In this condition, depolarization of the neuron from a state of hyperpolarized quiescence to continuous firing through the injection of DC current (see arrows for specific values) does not reveal a slow oscillation. After washout of LY367385, the neuron spontaneously depolarizes again and recovers its capacity to exhibit a slow oscillation (***A*$_3$**). The sections marked by continuous bars are expanded on the right. ***B***, Effect of tetanically stimulating CT fibers in an NRT neuron from the PGN at levels of initial membrane potential close to −75 mV (***B*$_1$**). At −74 mV, the poststimulus response is an isolated, long-lasting self-sustained up state (top trace). At −76 mV, this initial up state is shorter and is followed by a second spontaneous up state, thus leading to a brief slow oscillation (second trace from the top). A similar effect is observed at −77 mV, where a transient slow oscillation comprising three consecutive up states is apparent (third trace from the top). At −80 mV, CT stimulation leads to a long lasting EPSP (bottom trace) [compare Hughes et al. (2002a), their Fig. 5]. The generation of stimulus-dependent up states and the slow EPSP are both abolished by LY367385 (250 μM) (***B*$_2$**). Note, in the absence of CT stimulation, this neuron was unable to generate a slow oscillation or any type of spontaneous self-sustained up states. ***C***, Two consecutive responses (left and right traces) of an NRT neuron in the PGN to tetanic CT and thalamic stimulation show that the mGluR1a-dependent slow EPSP is a specific response to activating the CT pathway. ***D***, Histograms summarizing the properties of the poststimulus response at −80 mV after CT stimulation in control conditions (Con) and in the presence of LY367385 (LY), and after thalamic stimulation (Thal) (**$p < 0.01$; $n = 5$). In both ***B*** and ***C***, the stimulus protocol consisted of 25 pulses of 300 μA lasting 0.2 ms delivered at 50 Hz. CNQX (10 μM), APV (50 μM), SR95531 (20 μM), and CGP54626 (20 μM) were present in the recording medium for the experiments depicted in ***B–D***. Error bars indicate SE.

of any DC current, all cells displayed continuous tonic firing (Fig. 1*B*$_1$, top trace, 0 pA) (37.8 ± 4.3 Hz; $n = 42$). *Trans*-ACPD also led to a 25% rise in R_N (162.7 ± 10.4 MΩ; $n = 42$) (Fig. 1*B*$_2$).

In addition to responding to *trans*-ACPD with a robust depolarization and increase in R_N, a substantial proportion of NRT neurons also became able to generate a slow (<1 Hz) membrane potential oscillation ($n = 27$ of 61; 44%) (Fig. 1*B*$_1$, middle trace, −410 pA) (Crunelli et al., 2005) when they were hyperpolarized via the injection of DC current. This slow oscillation was manifested as alternating up and down states of the membrane potential that were separated by ~10–15 mV. During the up state, NRT neurons displayed sustained tonic firing, whereas during the down state, these cells were quiescent and often exhibited a slow sag-like depolarization (Fig. 1*B*$_1$). The transition from up to down state was typically characterized by a clear inflection point in the membrane potential, whereas the switch from down to up state was punctuated by the presence of one or more LTCPs and accompanying bursts of action potentials (see below) (Fig. 1*B*$_1$). The frequency of the slow oscillation ranged from 0.02–0.7 Hz with a mean minimum frequency across a population of cells of 0.16 ± 0.04 Hz ($n = 20$). A higher R_N was associated with the ability to display a slow oscillation (oscillating neurons: R_N = 156.7 ± 14.3 MΩ, $n = 16$; nonoscillating neurons: R_N = 132.0 ± 24.9 MΩ, $n = 21$), although this was not found to be statistically significant ($p = 0.26$). No major differences in the incidence of the slow oscillation were observed between different sectors of the NRT (PGN: 18 of 37, 49%; peri-VB sector: $n = 7$ of 18, 39%; peri-VL sector: $n = 2$ of 6, 33%).

The *trans*-ACPD-induced slow oscillation formed part of a continuum of activity patterns in NRT neurons being present only for a specific range of DC current values (Fig. 2*A*$_2$–*A*$_4$,*B*$_2$–*B*$_4$). With hyperpolarization below this range, the slow oscillation was sometimes replaced by rhythmic LTCPs at δ frequencies (1–4 Hz) ($n = 4$) (Fig. 2*A*$_1$,*B*$_1$) (Amzica et al., 1992) before a quiescent hyperpolarized membrane potential was reached (Fig. 2*A*). In contrast, depolarization above the DC current range for which the slow oscillation was present led to continuous tonic firing (Fig. 2*A*$_5$,*B*$_5$). To investigate whether mGluR activation was able to naturally bring about a slow oscillation in the absence of intracellular DC current injection, we performed extracellular recordings of

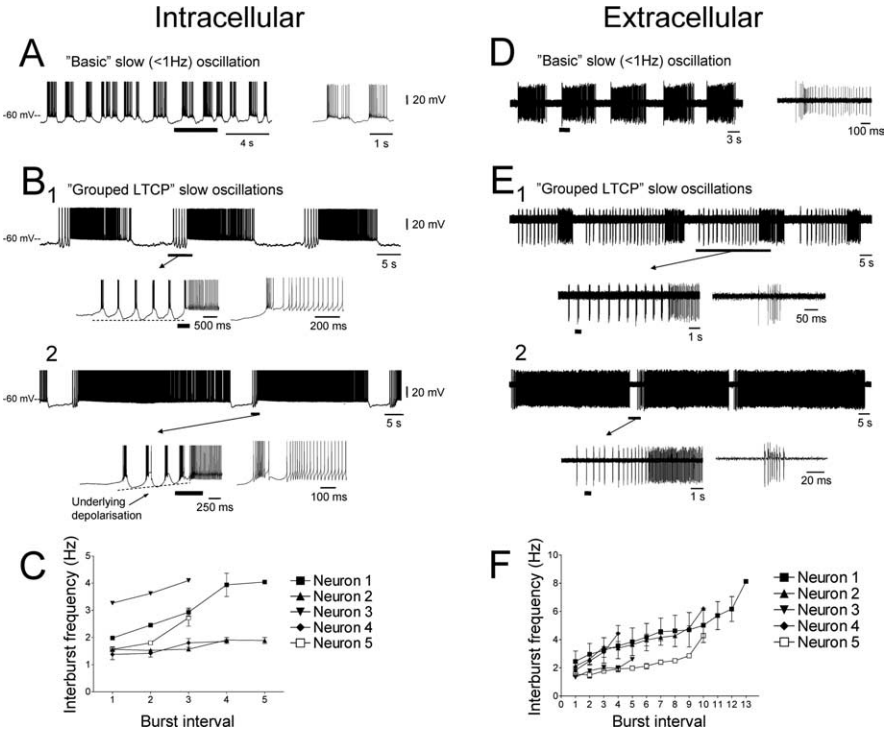

Figure 4. Different manifestations of the slow (<1 Hz) oscillation in NRT neurons. ***A***, Intracellular recording of an NRT neuron in the peri-VL sector in the presence of *trans*-ACPD (100 μM) displaying a basic slow oscillation. In this neuron, the slow oscillations were always of this type, regardless of the level of DC current. The underlined section is expanded on the right. ***B*$_1$**, Intracellular recording of a peri-VB-sector neuron in the presence of *trans*-ACPD (100 μM) displaying a slow (<1 Hz) oscillation that groups rhythmic LTCP bursting at ~1–2 Hz before the transition to the up phase. The underlined section is expanded below with the further marked section enlarged on the right. ***B*$_2$**, Intracellular recording of a PGN neuron in the presence of *trans*-ACPD (100 μM), which also exhibits rhythmic sequences of LTCP bursts before the commencement of the up state. The underlined section is expanded below and reveals that there is a clear increase in interburst frequency in the LTCP sequence as it progresses, which is associated with an unambiguous underlying depolarization. The trace on the right is an enlargement of one of the underlined bursts. ***C***, Plot showing the mean interburst frequency of successive bursts in five different NRT neurons that displayed the grouped LTCP subtype of the slow oscillation (3 cycles of the oscillation at the most positive level of DC current for which grouped episodes existed were used for this analysis). In each case, the interburst frequency increased during the grouped episodes. Neuron 1 corresponds to the neuron shown in ***B*$_2$** and neuron 2 is that depicted in ***B*$_1$**. ***D***, ***E***, Examples of the different manifestations of the slow oscillation as observed with extracellular recordings in the presence of 50 μM *trans*-ACPD. ***F***, Plot showing the mean interburst frequency of successive bursts in five different NRT neurons that displayed the grouped LTCP subtype of the slow oscillation in extracellular recordings. In all cases, the interburst frequency increased during the grouped episodes and was generally higher than that observed in intracellular recordings. CNQX (10 μM), APV (50 μM), SR95531 (20 μM), and CGP54626 (20 μM) were present in the recording medium for these experiments. Error bars indicate SE.

NRT neurons while closely scrutinizing the effect of *trans*-ACPD on their mode of activity. In control conditions, the majority (n = 27 of 46; 59%) of extracellular recordings displayed a lack of spontaneous activity (supplemental Fig. 1*A*$_1$, available at www.jneurosci.org as supplemental material). The remainder comprised either rhythmic LTCP-mediated bursts at δ frequencies (1.3 ± 0.1 Hz; n = 10), low-frequency tonic firing (4.1 ± 1.0 Hz; n = 5), or a spontaneous slow oscillation (0.14 ± 0.05 Hz; n = 4). When recording from sites that initially lacked any firing, application of *trans*-ACPD led to a progressive increase in activity, which always culminated in continuous tonic firing (supplemental Fig. 1A$_4$, available at www.jneurosci.org as supplemental material). However, while passing between a state of no activity and tonic firing, the majority (n = 16 of 27; 59%) of NRT neurons transiently displayed a slow oscillation (supplemental Fig. 1*A*$_3$, available at www.jneurosci.org as supplemental material). In some cases (n = 4), the slow oscillation was preceded by rhythmic LTCP-mediated bursts at δ frequencies (supplemental Fig. 1*A*$_2$, available at www.jneurosci.org as supplemental material) so that *trans*-ACPD application was able to elicit the full repertoire of NRT behavior observed with intracellular recordings (Fig. 2). In circumstances in which extracellular NRT recordings did not exhibit a slow oscillation during *trans*-ACPD application, we observed a direct transition from quiescence to tonic firing (n = 11 of 27; 41%) (data not shown). Thus, at appropriate intensities of mGluR activation, a slow oscillation constitutes the normal activity of a large proportion of NRT neurons. Indeed, application of a lower concentration of *trans*-ACPD (50 μM) led to a sustained slow oscillation being present in 59% (n = 16 of 27) of extracellular recordings (see Figs. 4*D*,*E*, 6*B*).

The action of *trans*-ACPD in bringing about a slow oscillation in NRT neurons was mimicked by the group I selective mGluR agonist, DHPG (100 μM). When assessed with intracellular recordings, addition of DHPG was associated with a tonic depolarization beyond the action potential threshold (mean frequency of tonic firing, 13.7 ± 5.5 Hz; n = 6) and a pronounced increase in R_N (control, 110.1 ± 16.4 MΩ; DHPG, 142 ± 12.2 MΩ; n = 6), with a slow oscillation being evident after steady hyperpolarization in 50% of neurons (n = 3 of 6). During extracellular recordings, DHPG application induced a change from quiescence to tonic firing in all cases (n = 10), with this transition occurring via a slow oscillation in 80% of recordings (n = 8 of 10) (supplemental Fig. 2*A*, available at www.jneurosci.org as supplemental material). The effects of *trans*-ACPD and DHPG observed with extracellular recordings were prevented when the mGluR1a-specific antagonist, LY367385 (250 μM), was included in the recording medium (n = 4) (data not shown), suggesting that the ability of NRT neurons to generate a slow oscillation was dependent on the specific activation of mGluR1a. This was confirmed by intracellular recordings showing that the capacity to produce a slow oscillation after *trans*-ACPD application was consistently and reversibly blocked by LY367385 (250 μM) (Fig. 3*A*) (n = 3 of 3).

To test whether the synaptic activation of mGluRs could also induce a slow oscillation, we examined the response of NRT neurons in the PGN to the tetanic stimulation of corticothalamic (CT) fibers. When neurons were held at an initial membrane potential close to −75 mV, a substantial proportion (n = 4 of 9; 44%) exhibited self-sustained up states after the offset of the stimulus epoch that could last for several seconds (5.7 ± 2.8 s; n = 4) (Fig. 3*B*$_1$) and which were similar to those observed spontaneously during the agonist-induced slow oscillation. Furthermore, in some cases these initial stimulus-induced up states could be closely ensued by one or two additional up states, thus constituting a slow oscillation (mean frequency, 0.14 ± 0.03 Hz; n = 4). When neurons were hyperpolarized to approximately −80 mV, the generation of up states no longer occurred in response to CT

stimulation. Instead, in this condition the poststimulus response was a long-lasting, slow EPSP (peak amplitude, 5.0 ± 0.5 mV; duration, 12.1 ± 2.5 s; $n = 4$) (Fig. 3B_1, bottom trace, D). Both, the stimulus-induced up states and the slow EPSP were suppressed by LY367385 (250 μM) ($n = 3$) (Fig. 3B_2,D). Thus, the effects of exogenously activating mGluR1a in bringing about a membrane depolarization and slow oscillation can also be achieved via a physiological release of glutamate after the stimulation of CT fibers. Notably, however, a similar effect was not attainable after tetanic stimulation of the thalamocortical pathway after placement of a stimulating electrode in lamina A of the LGN (Fig. 3C,D).

Analysis of the different manifestations of the slow (<1 Hz) oscillation in NRT neurons and their modification by membrane polarization

As already indicated, the essential appearance of the slow oscillation comprised the rhythmic alternation of distinct up and down membrane potential states with the up state supporting intense action potential firing in every case (see Figs. 1–7; supplemental Figs. 1, 2, 4, available at www.jneurosci.org as supplemental material). This firing generally decelerated as the up state progressed from a maximum frequency of 50.1 ± 8.5 Hz (range, 6.5–125 Hz; $n = 16$) at the start of the up state to a minimum of 9.4 ± 1.4 Hz (range, 2.3–18.1 Hz; $n = 16$) at its end. In 70% of intracellular and 62% of extracellular ($n = 19$ of 27 and $n = 20$ of 32, respectively) recordings, the switch from down to up state was always marked by the generation of a single LTCP-mediated burst of action potentials ("basic" slow oscillation) (Figs. 2, 4A,D; supplemental Fig. 2, available at www.jneurosci.org as supplemental material). This was true regardless of the DC current level or oscillation frequency. However, the remainder of cells (intracellular, $n = 8$ of 27, 30%; extracellular, $n = 12$ of 32, 38%) could exhibit a group of rhythmic LTCP-mediated bursts at this transition point ("grouped LTCP" slow oscillation) (Figs. 4B,E, 5B, 6C; supplemental Fig. 1, available at www.jneurosci.org as supplemental material). In some cases, these burst sequences were so pervasive that they essentially replaced the down state of the slow oscillation (Figs. 4E_1, 5B; supplemental Fig. 1, available at www.jneurosci.org as supplemental material). Rhythmic burst sequences occurred at a range of frequencies (1.3–8.2 Hz; $n = 10$) that encroaches on both the δ (1–4 Hz) and sleep spindle (7–14 Hz) frequency bands, with the precise interburst frequency usually ($n = 18$ of 20; 90%) increasing as the sequence progressed (Fig. 4C,F). In some neurons, this increase was subtle (Fig. 4B_1), whereas in other cells, the increase was more conspicuous and associated with an obvious, underlying depolarizing envelope in intracellular recordings (Fig. 4B_2).

The overall frequency of the basic manifestation of the slow oscillation in NRT neurons decreased with depolarization (Figs. 2, 5). This occurred through a gradual increase in the duration of the up state and the consequential steady decline in the incidence of a down state, the properties of which were largely insensitive to membrane polarization (Fig. 5A). For slow oscillations involving grouped LTCP episodes, depolarization also caused an increase in the duration of the up state. However, in these oscillations, the down state could also be dynamic. This was especially true in the initial stages of depolarization, where a reduction in the number of LTCP-mediated bursts and an increase in their interburst frequency were often observed (Fig. 5B). The sensitivity of the properties of rhythmic LTCP burst sequences to membrane polarization meant that the relationship between DC current and slow oscillation frequency for grouped LTCP slow oscillations was not straightforward, often exhibiting an initial increase followed by a clear decline (Fig. 5B_4).

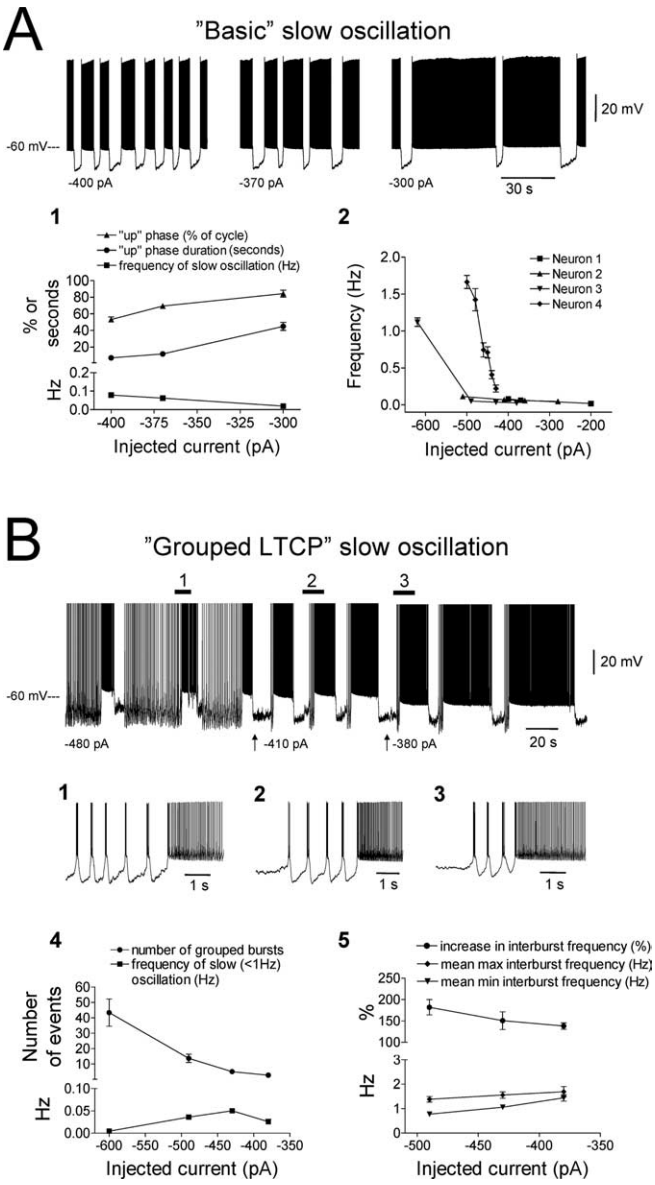

Figure 5. Dependence of the properties of the slow (<1 Hz) oscillation on membrane polarization. ***A***, Intracellular recording of an NRT neuron in the PGN in the presence of *trans*-ACPD (100 μM) displaying a basic slow oscillation only. The frequency of the oscillation decreases as the neuron is depolarized, an effect that is caused by a progressive increase in the duration of the up state (***A*$_1$**). The lower right plots (***A*$_2$**) illustrate the variation in frequency of the basic slow oscillation with respect to DC current in four NRT neurons. ***B***, NRT neuron in the PGN recorded in the presence of *trans*-ACPD (100 μM) displaying a grouped LTCP slow oscillation (top trace). The sections marked ***1***, ***2***, and ***3*** are expanded below. As with the basic oscillation, the up state shows a progressive increase in duration with increasing depolarization. However, the down state is also dynamic, showing a steady decrease in length and number of LTCP-bursts in each oscillation cycle as the neuron is depolarized (***B*$_4$**). This leads to a more complex relationship between oscillation frequency and DC current (***B*$_4$**). The lower right plots (***B*$_5$**) illustrate the variation in the properties of the rhythmic LTCP burst sequences as the DC current is increased. Action potentials have been truncated in ***B***. Error bars indicate SE.

The slow (<1 Hz) oscillation is resistant to blockade of Na^+ channels

The slow oscillation in NRT neurons is dependent on intrinsic ionic mechanisms because it was routinely observed in the presence of blockers of ionotropic glutamate, $GABA_A$, and $GABA_B$

receptors (CNQX, 10 μM; APV, 50 μM; SR95531, 20 μM; CGP54626, 20 μM; $n = 12$) (Figs. 4*D*,*E*; supplemental Figs. 1, 2, available at www.jneurosci.org as supplemental material). The slow oscillation was also resistant to the application of TTX (1 μM) ($n = 4$ of 4) (Fig. 6*A*), suggesting that (1) it arises as a direct activation of postsynaptic mGluR1a receptors, (2) it is not reliant on Na^+ channels, and (3) it does not require an Na^+-activated K^+ current ($I_{K(Na)}$) (Kim and McCormick, 1998; Bhattacharjee and Kaczmarek, 2005). TTX did, however, cause a clear decrease in the duration of the down state (15.8 ± 6.6 vs 5.3 ± 0.3 s; $n = 4$; $p < 0.1$) (Fig. 6*A*), an effect that might be related to a secondary inhibition of $I_{K(Na)}$ (Fig. 9B_4).

In TC neurons, the instatement of a slow oscillation only occurs when I_{Leak} is reduced below a specific threshold (Williams et al., 1997; Tóth et al., 1998; Hughes et al., 1999). To test whether some NRT neurons lack a slow oscillation because mGluR1a activation in these cells does not sufficiently reduce I_{Leak}, we artificially induced a further suppression of this current using a dynamic-clamp system in non-oscillating NRT neurons that had been subjected to TTX (Hughes et al., 1999, 2002a) (supplemental Fig. 3*A*, available at www.jneurosci.org as supplemental material). In all cases ($n = 3$ of 3), for a certain level of additional artificial I_{Leak} reduction (−5.2 ± 0.5 nS), we were able to induce a slow oscillation (Fig. 3*B*). Thus it appears that the ability to generate a slow oscillation is a general property of NRT neurons, which becomes evident when I_{Leak} is reduced below a particular threshold.

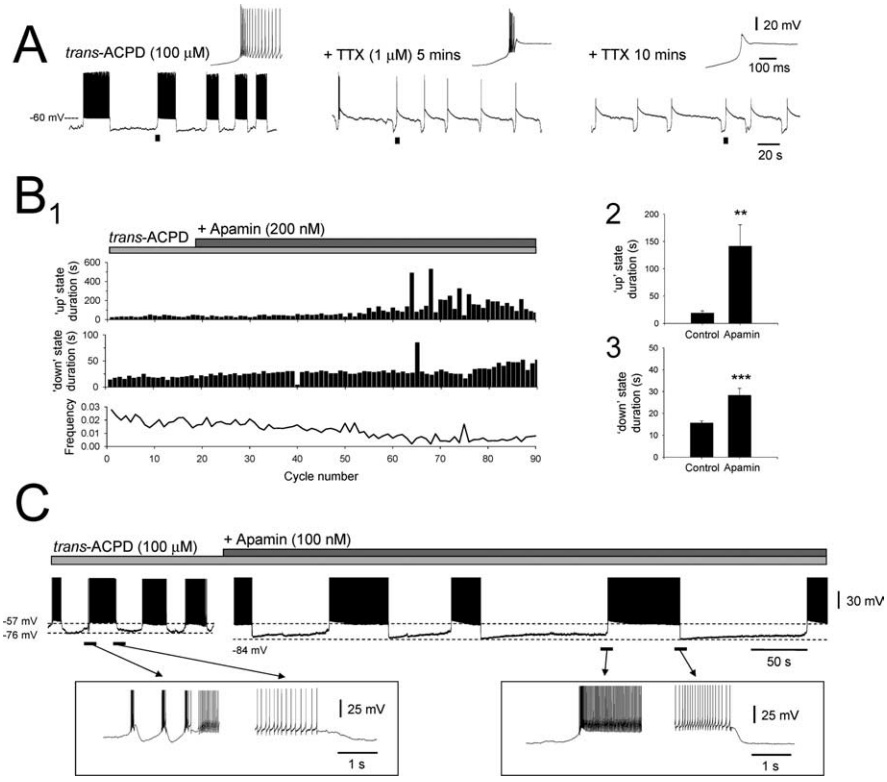

Figure 6. Lack of involvement of Na^+ channels and the role of $I_{K(Ca)}$ in the slow (<1 Hz) oscillation. ***A***, Intracellular recording of an NRT neuron in the PGN in the presence of *trans*-ACPD (100 μM) displaying a basic slow oscillation (left trace). Five minutes after applying TTX (1 μM), the intense firing on the up state is abolished, although a burst of action potentials remains at the commencement of each up state (middle trace). After 10 min, TTX blocks all action potentials but the slow oscillation remains intact (right trace). Note the decrease in the duration of the down state that occurs with TTX treatment. In each panel, underlined sections are enlarged on the top right. ***B_1***, Summary of the effect of apamin (200 nM) on the properties of a slow oscillation recorded extracellularly from an NRT neuron in the peri-VL sector (recorded in the presence of 50 μM *trans*-ACPD). Apamin causes a dramatic decrease in oscillatory frequency (bottom plot), which is brought about by a progressive lengthening of both the up (top plot) and down state (middle plot). ***B_2–B_3***, Histograms summarizing the effect of 200 nM apamin on the duration of the up (***B_2***) and down (***B_3***) states in 3 NRT neurons recorded extracellularly in the presence of 50 μM *trans*-ACPD (**$p < 0.01$; ***$p < 0.001$; $n = 6$). ***C***, Intracellular recording from an NRT neuron in the peri-VL sector in the presence of *trans*-ACPD (100 μM) displaying a grouped LTCP slow oscillation (left). The underlined sections are expanded below. Application of apamin (100 nM) causes a dramatic increase in the oscillation period, which is associated with an augmentation in the duration of both the up and down state (right). Apamin also abolishes the rhythmic LTCP sequence that precedes the commencement of the up state and increases the extent to which the neuron hyperpolarizes during the down state (see enlargements below). Note also the increased evidence of a slow depolarization during the down state and the increased steepness of the up to down state transition after apamin treatment (compare Fig. 9 *A*, *C*). Action potentials have been truncated in this figure. Error bars indicate SE.

Blocking Ca^{2+}-activated K^+ channels with apamin dramatically lengthens the period of the slow (<1 Hz) oscillation

NRT neurons possess a prominent Ca^{2+}-activated K^+ current ($I_{K(Ca)}$), which profoundly influences the electroresponsiveness of these cells (Bal and McCormick, 1993). To investigate whether $I_{K(Ca)}$ plays a role in determining the properties of the slow oscillation, we assessed the effect of the SK channel blocker apamin on NRT neurons exhibiting this activity. When apamin (200 nM) was applied during extracellular recordings of spontaneous slow oscillations that had been induced by 50 μM *trans*-ACPD (see above), we consistently observed a dramatic decrease in the frequency of the oscillation (0.02 vs 0.006 Hz; $n = 6$). This decrease was brought about by a progressive lengthening of both the up (18.9 ± 4.2 vs 141.3 ± 40.5 s; $n = 6$; $p < 0.01$) and down states (15.6 ± 1.1 vs 28.3 ± 3.3 s; $n = 6$; $p < 0.001$) (Fig. 6*B*). Apamin also blocked the generation of grouped LTCP episodes, when they were present, such that after its application, all up states commenced with a single LTCP-mediated burst ($n = 2$) (data not shown). Intracellular recordings revealed a similar pattern to that observed extracellularly and showed that the lengthening of the oscillation period was also accompanied by a significant increase in the level of hyperpolarization reached during the down state (−76.7 ± 0.9 vs −86.3 ± 0.9 mV; $n = 4$; $p < 0.001$) (Fig. 6*C*).

The slow (<1 Hz) oscillation requires the activation of I_h

In most, although not all, instances of the slow oscillation, the down state was characterized by a slow or sag-like depolarization of the membrane potential (Figs. 1, 2, 3*A*, 4B_2, 5, 6*A*, 7*A*, top trace) (but see Figs. 4A,B_1, 6*C*, preapamin trace). A similar slow depolarization could also be observed in the voltage responses to large hyperpolarizing current steps illustrating that it is a fundamental property of NRT neurons (Fig. 7*A*, control in bottom traces) (Brunton and Charpak, 1997). The slow depolarization observed in response to large current steps was abolished by the potent and selective h-channel blocker ZD7288 (30 μM) (Bo-Smith et al., 1993) ($n = 8$) (Fig. 7*A*, ZD7288 in bottom traces). Predictably, block of the slow depolarization also led to neurons being unable to generate a slow oscillation ($n = 5$) (Fig. 7*B*). Importantly, this was true regardless of whether the down state of the slow oscillation exhibited an overt slow depolarization ($n =$

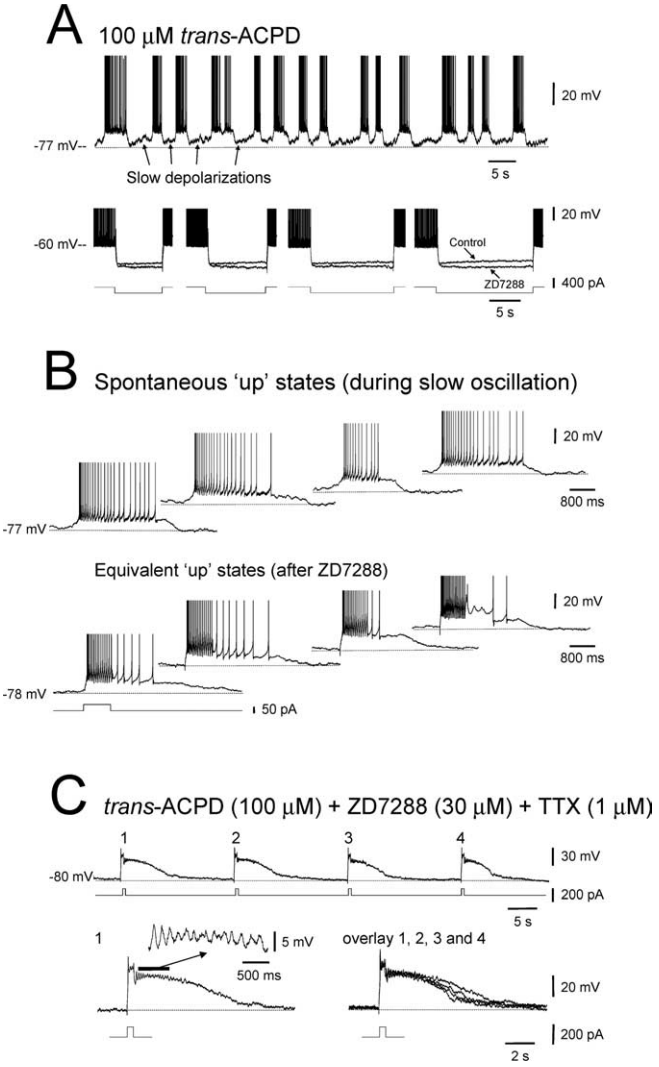

Figure 7. The slow depolarization during the down state of the slow (<1 Hz) oscillation is generated by I_h. ***A***, Slow oscillation recorded in the peri-VB sector in the presence of 100 μM *trans*-ACPD (top trace). Note the presence of slow depolarizations during the down state. The response of this neuron to large hyperpolarizing current steps was also characterized by slow depolarizations (bottom traces, control). These slow depolarizations were blocked by the potent and selective h-channel blocker ZD7288 (30 μM) (bottom traces, ZD7288). ***B***, After ZD7288 application, the slow oscillation in ***A*** is abolished. However, self-sustained equivalent up states (bottom set of traces), which were similar to those generated spontaneously during the slow oscillation (top set of traces), could still be elicited through the injection of brief depolarizing current pulses. ***C***, Equivalent up states are also present in TTX (recorded from an NRT neuron in the PGN). Note the presence of a clear membrane potential oscillation at ~6–8 Hz during the peak of the equivalent up state in this condition. Action potentials have been truncated in ***A*** and ***B***.

4) (Fig. 7*A*) or one that was more subtle ($n = 1$) (supplemental Fig. 4, available at www.jneurosci.org as supplemental material).

Although ZD7288 blocked the slow oscillation, self-sustained up states with similar properties to those observed spontaneously could still be triggered via the injection of brief depolarizing current steps (Fig. 7*B*). These events were termed equivalent up states. Thus, although a block of I_h leads to an elimination of the slow oscillation, the basic mechanism underlying the generation of each up state remains intact. Indeed, this mechanism can still be accessed through the injection of small current steps but it ceases to be recruited spontaneously. To further illustrate the lack of Na^+ channel involvement in the underlying mechanism of the slow oscillation, we assessed the effect of coapplying ZD7288 and TTX to NRT neurons exhibiting a slow oscillation. In this condition, NRT neurons were still able to generate clear equivalent up states when challenged with small depolarizing current steps ($n = 2$) (Fig. 7*C*). Interestingly, these equivalent up states were commonly characterized by a low amplitude (~3–6 mV from peak to peak) oscillatory activity (mean frequency, 8.4 ± 1.9 Hz; $n = 2$) (Fig. 7*C*).

The up state of the slow (<1 Hz) oscillation is dependent on T-type Ca^{2+} channels

In TC neurons, the mechanism underlying the generation of the up state in the slow oscillation relies critically on the window component of the T-type Ca^{2+} current (i.e., $I_{Twindow}$) (Crunelli et al., 2005). To test whether a similar mechanism might also be involved in the generation of up states in NRT neurons, we compared the effect of equal concentrations of Ni^{2+} and Cd^{2+} ions on the activity of slow oscillating NRT neurons that had been subjected to ZD7288. In doing so we were able to show that whereas application of Cd^{2+} (250 μM) ($n = 3$) was unable to block the generation of equivalent up states (Fig. 8*C*), Ni^{2+} (250 μM) caused a reversible abolition of these events in all cases ($n = 3$ of 3) (Fig. 8*A–C*) (Beurrier et al., 1999). Because Ni^{2+} is much more effective at blocking T-type Ca^{2+} channels than Cd^{2+} (Crunelli et al., 1989) this result strongly suggested that $I_{Twindow}$ might also be fundamental to the generation of the up state of the slow oscillation in NRT neurons. However, an alternative explanation is that the up state is generated purely by the action of a CAN current, which is activated by Ca^{2+} entry through T-type channels (Bal and McCormick, 1993; Destexhe et al., 1994), and which would, therefore, also be preferentially inhibited by Ni^{2+} rather than Cd^{2+}.

Computer simulations

To fully understand the mechanism of the slow oscillation, we constructed a biophysically realistic model of an NRT neuron. This model reliably recreated the main features of the slow oscillation including (1) a clear membrane potential inflection at the transition from up to down state, (2) a slow depolarization during the down state, (3) the presence of rhythmic LTCP burst sequences at the switch from down to up state for certain levels of DC current, and (4) decelerating tonic firing during the up state (Fig. 9*A*). Consistent with experimental results, the slow oscillation in the model did not require Na^+ channels (Fig. 9B_1–B_3). However, in similarity to the effect of TTX, a suppression of the transient Na^+ current led to a clear shortening of the down phase (8.0 s with $g_{Na} = 964$ nS vs 2.4 s with $g_{Na} = 0$ nS for a DC current of −50 pA) (compare Figs. 6*A*, 9*A*, 10B_2,B_3). Importantly, further excluding I_{CAN} from the model did not prevent a slow oscillation, although in this condition, the oscillation displayed a greatly reduced amplitude (12 vs 21 mV from peak to peak) (Fig. 9B_3). With I_{Na} and I_{CAN} reinstated to the model, specific inhibition of $I_{K(Na)}$ caused a decrease in the duration of the down state (Fig. 9B_4; compare Fig. 9*A*) that was equivalent to that observed when $g_{Na} = 0$ nS (Fig. 9B_2) (2.4 vs 2.6 s for a DC current of −50 pA). This suggests that the reduction in the length of the down state observed after TTX application in experiments is indeed caused by a secondary inhibition of $I_{K(Na)}$ (Fig. 6*A*). As in experiments, an inhibition of $I_{K(Ca)}$ (i.e., $g_{K(Ca)} = 0$ nS) caused both a lengthening of the slow oscillation period (15.0 vs 25.2 s for a DC current of −50 pA) and an augmentation of the level of hyperpolarization reached during the down state (−90 vs −78 mV) (Fig. 9*C*; compare Fig. 6*C*).

Regardless of the values of g_{Na}, $g_{K(Na)}$, and $g_{K(Ca)}$, and as ex-

pected from experiments, the model was unable to reproduce a slow oscillation when either I_T or I_h were absent. Also in line with our experimental results, during a simulated block of I_h, self-sustained equivalent up states could still be generated through the injection of brief depolarizing current pulses (Fig. 10*A*). In further accordance with experiments, these equivalent up states were resistant to the removal of I_{Na} (Fig. 10*B*) but abolished when I_T was absent (Fig. 10*C*). To test whether or not I_{CAN} is crucial for the generation of equivalent up states, the behavior of the model was scrutinized in the absence of this current (i.e., $g_{CAN} = 0$ nS). In this condition, equivalent up states could still be produced for certain values of DC current, albeit with a reduced duration (Fig. 10*D*). This is consistent with the finding that a slow oscillation can be still be generated in the absence of I_{CAN} (Fig. 10B_3) and further supports the hypothesis that equivalent up states are dependent on $I_{Twindow}$. To confirm this, we reinstated I_{CAN} to the model and specifically reduced $I_{Twindow}$ by shifting the steady-state inactivation curve of I_T by 3 mV in the negative direction (Fig. 10E_2, top plot). By performing this shift we ensured that the transient activation of I_T was essentially unchanged but that $I_{Twindow}$ was virtually eliminated (Hutcheon et al., 1994; Williams et al., 1997) (Fig. 10E_2, bottom plot). Under these conditions, the model was unable to generate equivalent up states (Fig. 10E_1). Importantly, for this set of simulations, we adjusted the equation governing the local intracellular Ca^{2+} processing ($\rho = 1.08 \times 10^{-4}$ nM · pA^{-1} · ms^{-1}) so that its time course (i.e., peak value and time to decay) after transient I_T activation matched that apparent for the control scenario (comparison not shown). This guaranteed that the time course of I_{CAN} also matched that occurring in control simulations and enabled us to be fully confident that the effect on voltage responses of shifting the steady-state inactivation curve of I_T was a consequence of reducing $I_{Twindow}$. Finally, when I_h was reintroduced to the model, we found that the 3 mV hyperpolarizing shift in the steady-state inactivation curve of I_T prevented a slow oscillation from being generated (data not shown). Thus, equivalent up states, and therefore the slow oscillation, are critically reliant on the presence of $I_{Twindow}$. A detailed summary of the ionic mechanisms of the slow oscillation in NRT neurons is given in supplemental Figure 5, available at www.jneurosci.org as supplemental material.

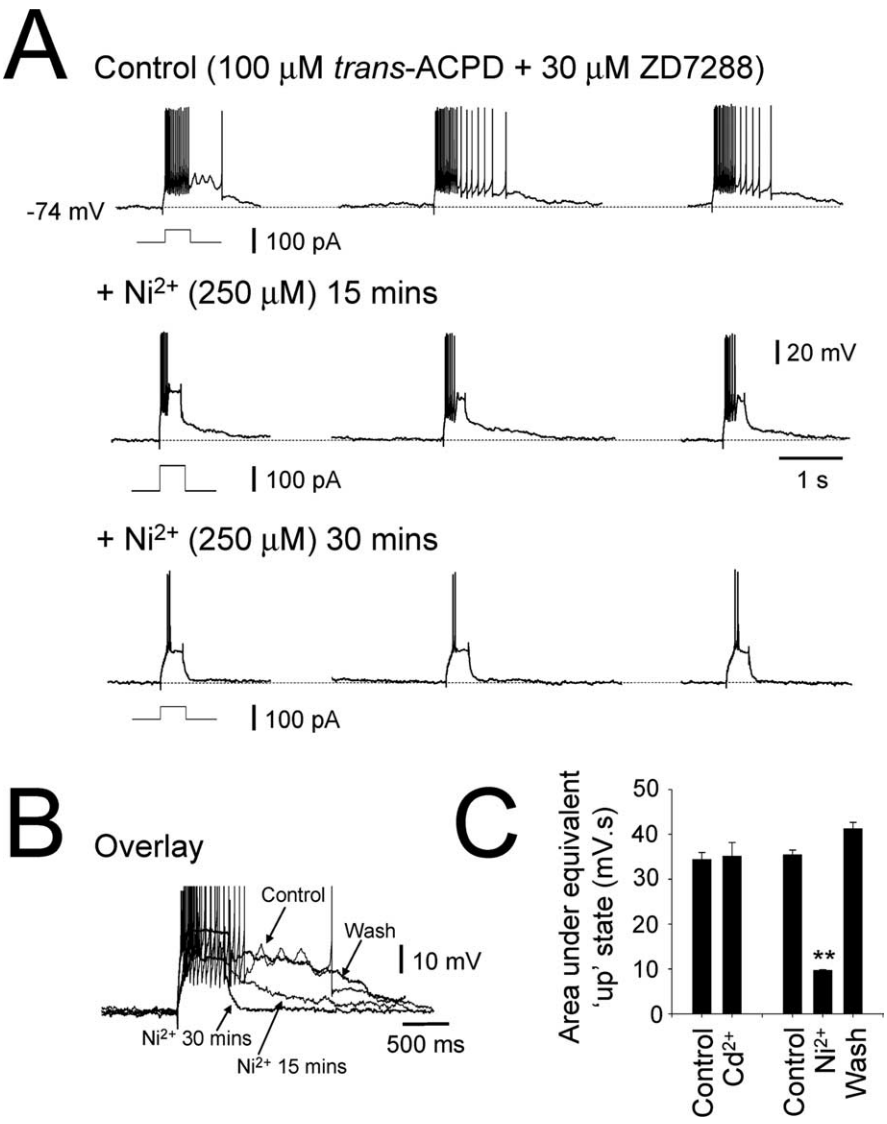

Figure 8. Equivalent up states are dependent on T-type Ca^{2+} channels. ***A***, Three consecutive equivalent up states recorded in the presence of 100 μM *trans*-ACPD and 30 μM ZD7288 (top traces) in a peri-VL sector neuron. Fifteen minutes after applying Ni^{2+} (250 μM), equivalent up states are substantially reduced, even when elicited by a current pulse that is twice the amplitude of that used in the control scenario (i.e., *trans*-ACPD plus ZD7288) (middle traces). After 30 min, Ni^{2+} abolishes equivalent up states in this neuron. ***B***, Overlay of typical responses to a small depolarizing current step showing the progressive block of the equivalent up state by Ni^{2+} and its subsequent recovery after washout. ***C***, Histogram summarizing and comparing the effects of Cd^{2+} (250 μM) (3 cells) and Ni^{2+} (3 cells) (250 μM) on equivalent up states in NRT neurons (**$p < 0.01$). Error bars indicate SE.

Discussion

The main findings of this study are (1) reduction of I_{Leak} via exogenous or synaptic activation of mGluR1a in NRT neurons *in vitro* leads to the instatement of an intrinsic slow (<1 Hz) oscillation with similar properties to those observed *in vivo* during deep sleep (Domich et al., 1986; Steriade et al., 1986) and certain types of anesthesia (Steriade et al., 1993c; Contreras and Steriade, 1995; Steriade et al., 1996; Timofeev and Steriade, 1996), (2) the slow oscillation is predominantly reliant on $I_{Twindow}$ and I_h, and (3) the properties of the slow oscillation are also influenced by the activity of a CAN current (I_{CAN}), a Ca^{2+}-activated K^+ current ($I_{K(Ca)}$) and an Na^+-activated K^+ current ($I_{K(Na)}$). This study is the first to expound the mechanisms of the slow oscillation in NRT neurons and endorses the idea that the slow (<1 Hz) sleep rhythm is actively shaped by the thalamus (Hughes et al., 2002a).

Comparison with the slow (<1 Hz) oscillation observed in NRT neurons *in vivo*

The slow oscillation in NRT neurons *in vitro* is qualitatively similar in several respects with that observed *in vivo* (Steriade et al.,

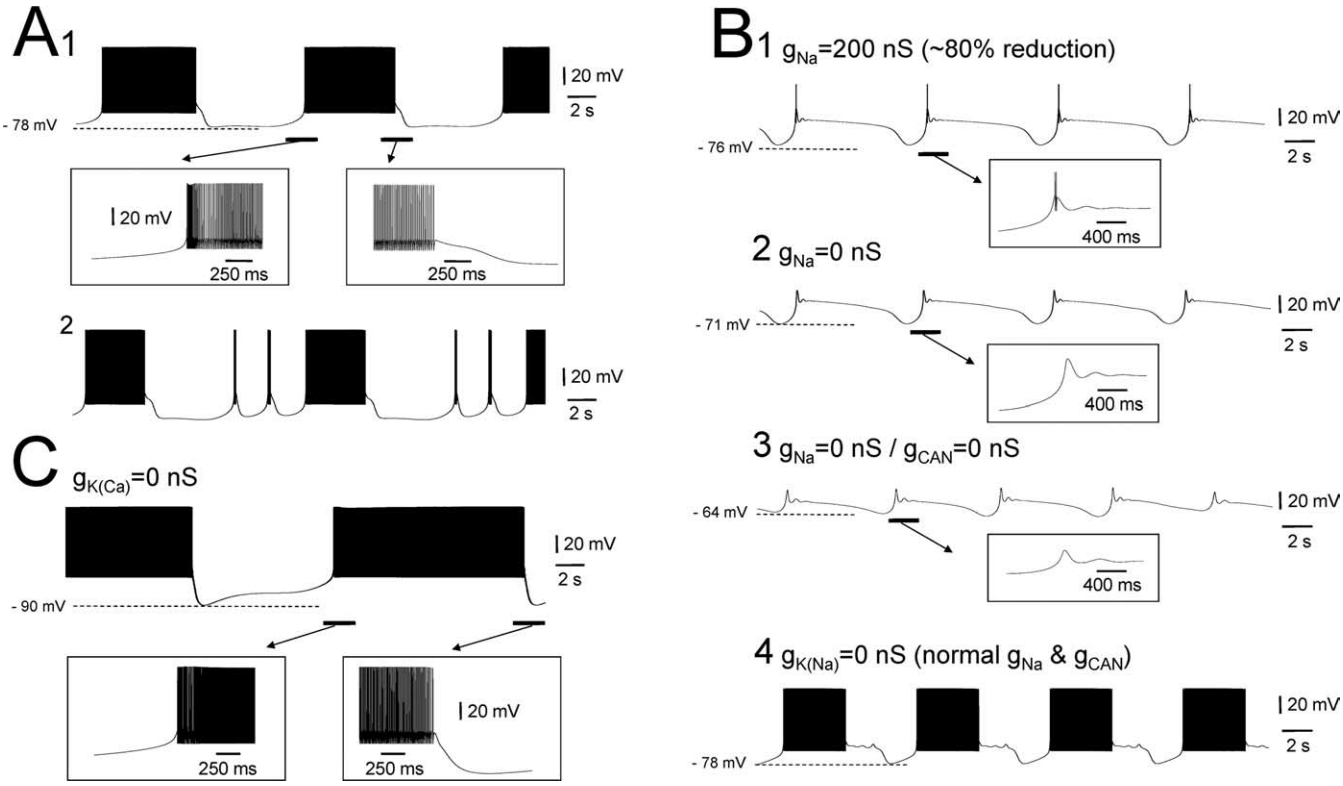

Figure 9. An NRT neuron model reproduces the main features of the slow (<1 Hz) oscillation. ***A*$_1$**, Example of the basic slow oscillation in an NRT neuron model (DC current is −50 pA). The underlined sections are expanded below (as indicated by the arrows) and show the similarity in the down to up and up to down state transitions with those observed during experiments. ***A*$_2$**, At a slightly more negative value of DC current (−57 pA), the model exhibits a grouped LTCP slow oscillation. ***B*$_1$**, A reduction in g_{Na} from 964 to 200 nS blocks tonic firing during the up state of the oscillation but leaves the action potentials comprising the burst at the beginning of the up state partially intact (enlarged inset). ***B*$_2$**, Full removal of I_{Na} from the model abolished all firing but does not eliminate the slow oscillation (enlarged inset). Note the clear decrease in the duration of the down state in ***B*$_1$** and ***B*$_2$** in comparison to ***A*$_1$** (compare Fig. 6*A*). ***B*$_3$**, Exclusion of I_{CAN} from the model does not impede the generation of the slow oscillation but greatly reduces its peak to peak amplitude. ***B*$_4$**, Specific removal of $I_{K(Na)}$ from the model without interfering with I_{Na} and I_{CAN} causes a decrease in the duration of the down state, which is equivalent to that induced when $g_{Na} = 0$ nS (DC current is −50 pA for ***B*$_1$**–***B*$_4$**). ***C***, Removal of $I_{K(Ca)}$ from the model increases the oscillation period, enhances the level of hyperpolarization reached during the down state and makes the slow depolarization that is present during the down state more evident (DC current same as ***A*$_1$**, i.e., 50 pA). The underlined sections are expanded below (as indicated by the arrows). Note the increase in steepness of the up to down state transition compared with ***A*$_1$** (compare Fig. 6*C*).

1993c, 1996; Contreras and Steriade, 1995; Timofeev and Steriade, 1996). First, both the *in vitro* and *in vivo* slow oscillations comprise a regular, stereotypical alternation between distinct up and down membrane potential states. Second, the full stereotypical expression of the slow oscillation is dependent on membrane polarization in both conditions. Third, the commencement of the up state in each context is often marked by the generation of one or more clear LTCP-mediated bursts. Fourth, the up state in both scenarios is characterized by intense, sustained action potential firing. Fifth, the transition from the up to down state in both cases is frequently initiated by a stereotypical inflection point of the membrane potential. Despite these qualitative similarities, the frequency of the slow oscillation *in vivo* (typically ~0.3–0.5 Hz) is generally somewhat higher than that observed *in vitro* (~0.05–0.5 Hz). This suggests that the intrinsic slow oscillation in NRT neurons does not greatly dictate the frequency of network oscillations in the whole brain. Rather, it is likely that, *in vivo*, the up and down states inherent to NRT neurons are recruited by external influences (i.e., predominantly from the cortex) (Steriade et al., 1993b; Sanchez-Vives and McCormick, 2000) but probably also from TC neurons (Steriade et al., 1993c; Hughes et al., 2002), and entrained into a faster oscillatory activity than occurs naturally in these cells. Alternatively, $I_{K(Ca)}$ and $I_{K(Na)}$, which play a significant role in determining slow oscillation frequency (see below) might be differentially regulated *in vivo*. Either way, intrinsic up and down states in NRT neurons endow these cells with the ability to "resonate" within the frequency of slow waves, which in turn would actively reinforce ongoing network oscillations.

A role for various neurotransmitters in supporting the slow oscillation

A recent *in vitro* study has shown that thyrotropin-releasing hormone (TRH) is also able to bring about a slow oscillation in NRT neurons (Broberger and McCormick, 2005) with similar properties to those shown here and by us previously (Crunelli et al., 2005). Because TRH and mGluR agonists both decrease I_{Leak} in NRT neurons, it appears that the slow oscillation is a latent property of these cells *in vitro* that can be supported by the activation of several different neuromodulatory pathways that are active *in vivo* and which target this current. Consistent with this, decortication, a procedure that eliminates the cortical mGluR pathway to the thalamus, drastically reduces the proportion of NRT neurons that exhibit a slow oscillation *in vivo* (to 8%) (Timofeev and Steriade, 1996), a finding that fits well with our experiments showing that electrical stimulation of corticothalamic fibers *in vitro* can bring about a slow oscillation via mGluR1a activation. That a small amount of NRT neurons *in vivo* still generate a slow oscillation after decortication is paralleled by our finding that a minority of NRT neurons recorded extracellularly *in vitro* demonstrate a spontaneous slow oscillation in control conditions (9%), and is also coherent with activation of other receptors apart

from mGluR1a being able to induce this activity. Nevertheless, for the slow oscillation to be present to any great extent in NRT neurons *in vivo*, an intact cortical input appears to be necessary. This ultimately points to the cortex as having primary responsibility for initiating the slow rhythm, a proposal backed up by its presence *in vivo* after thalamectomy (Steriade et al., 1993b).

The ionic basis of the slow (<1 Hz) oscillation in NRT neurons

Although not demonstrating a spontaneous slow oscillation, a previous *in vitro* investigation has highlighted the ability of NRT neurons to generate intrinsic plateau potentials, which are similar to the equivalent up states shown here (Kim and McCormick, 1998). However, at odds with our results is the finding that these plateau potentials are dependent on persistent Na^+ channels. Interestingly, a recent *in vivo* study has also ascribed a role for a persistent Na^+ current in the generation of plateau potentials in NRT neurons (Fuentealba et al., 2005). In our study, TTX did not block either the slow oscillation or equivalent up states. However, TTX did initially cause a specific block of tonic action potential firing during the up state while sparing the action potentials comprising the bursts marking the transition between the down and up state. Our initial suspicion was that this was because of a preferential block of persistent Na^+ channels by TTX (Tennigkeit et al., 1998). However, a similar result was obtained in the model, where a reduction of transient Na^+ current mimicked the early effect of TTX. Thus, a persistent Na^+ current plays no role in the slow oscillation in NRT neurons. Rather, both experiments and modeling show that equivalent up states, and therefore the slow oscillation, are primarily dependent on $I_{Twindow}$.

A common, although not ubiquitous, feature of the slow oscillation was a slow or sag-like depolarization during the down phase. Because this was also present after TTX treatment, it could not be attributed to an Na^+-activated K^+ current (Kim and McCormick, 1998; Bhattacharjee and Kaczmarek, 2005). Rather, it is caused by an I_h current because it was consistently blocked by the selective h-channel blocker, ZD7288 (BoSmith et al., 1993). This is consistent with the observation of similar sag-like potentials in NRT neurons by others (Brunton and Charpak, 1997; Zhang and Jones, 2004), and with the intense localized expression of the HCN2 subunit, and moderate expression of the HCN3 and HCN4 subunits, in the rat NRT (Monteggia et al., 2000; Notomi and Shigemoto, 2004). In all cases, blocking the slow depolarization with ZD7288 also eliminated the slow oscillation demonstrating that I_h is crucial to this activity. An identical result was obtained when I_h was removed from our computational model.

Although not central to slow oscillation generation, $I_{K(Ca)}$ plays an important role in controlling its frequency because apamin caused a substantial increase in the duration of both the up and down states. After apamin treatment, it also became much easier to observe a slow depolarization during the down state. This is important because in some instances of the slow oscillation, a clear slow depolarization was not evident. However, one such oscillation was still abolished by the h-channel blocker ZD7288, suggesting that I_h is active in cells lacking an obvious slow depolarization but that its effect is partially occluded. Such occlusion may be attributable to the presence of a large $I_{K(Ca)}$ in these cells, which has a shunting effect during the down state.

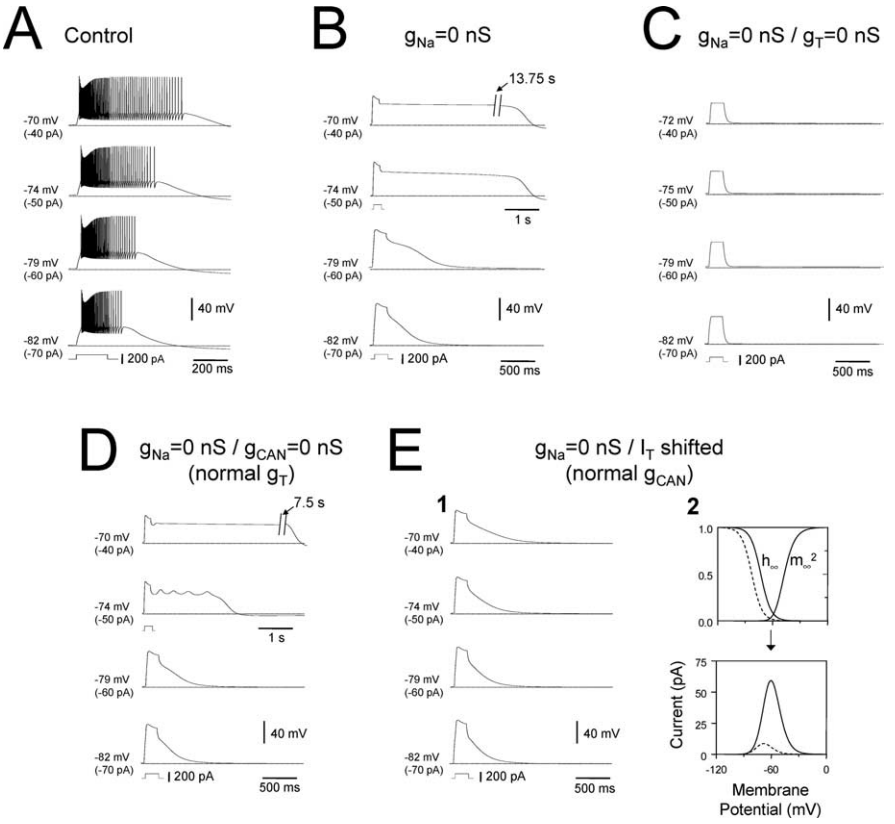

Figure 10. Confirmation that $I_{Twindow}$ is necessary for the up state of the slow (<1 Hz) oscillation. ***A***, After a simulated block of I_h, the model exhibits self-sustained equivalent up states that are similar to those observed in experiments (compare Fig. 7*B*). Each trace depicts the response to a 100 pA current pulse of 200 ms duration. The different DC current values and corresponding membrane potentials are indicated on the left of each trace. Note that the length of equivalent up states increases as the neuron is depolarized, consistent with the experimental observation that the up state of the slow oscillation increases in duration as NRT neurons are depolarized (Fig. 5). ***B***, An equivalent set of simulations performed with $g_{Na} = 0$ nS show that equivalent up states are not dependent on Na^+ channels. Indeed, equivalent up states appear to be enhanced in this condition (compare Fig. 7*C*). The equivalent up state in the top trace lasts for several seconds as illustrated by the break in the trace. ***C***, Equivalent up states are absent when $g_T = 0$ nS (compare Fig. 8*A*, bottom set of traces). ***D***, The same simulations performed after the removal of I_{CAN}, but with normal I_T parameters, exhibit robust equivalent up states. Again, the equivalent up state in the top trace lasts for several seconds. ***E***, Reinstatement of I_{CAN} to the model while shifting the steady-state inactivation curve of I_T by 3 mV in the negative direction abolishes equivalent up-state production (***E*** $_1$). Rather than displaying equivalent up states, these simulations show a small, slowly decaying depolarization after the offset of depolarizing current steps, which is presumably caused by a simple combination of slow I_T inactivation (Huguenard and Prince, 1992) and I_{CAN}. The effect of shifting steady-state inactivation is schematically illustrated on the right (***E*** $_2$). The continuous lines in the top plot represent the normal steady-state inactivation (h_∞) and activation (m_∞^2) functions. The substantial overlap in these curves leads to an appreciable window current (i.e., $I_{Twindow}$) (continuous line in bottom plot). However, after h_∞ is shifted (dotted line in top plot), the region of overlap and, consequently, $I_{Twindow}$ (dotted line in bottom plot) are greatly reduced.

Consistency with previous *in vitro* studies and a proposed role for electrical synapses in synchronizing the NRT slow oscillation

A recent study using slices from young rats has also examined the effects of mGluR activation on NRT neurons (Long et al., 2004). In this investigation, the authors describe the appearance of subthreshold membrane potential oscillations at ~10 Hz. Although

under normal conditions we did not see similar activity in our study, oscillations at close to 10 Hz were sometimes observed during equivalent up states recorded in the presence of TTX. This suggests that while not being overt under normal conditions, a 10 Hz oscillation is still present in cat NRT neurons and might influence firing rate during the slow oscillation up state. The 10 Hz oscillation described by Long et al. (2004) was synchronized between closely situated cells via electrical synapses (Landisman et al., 2002). Because evidence for electrical synapses is present in recordings from NRT neurons in the adult cat *in vivo* (Fuentealba et al., 2004), the possibility exists that electrical synapses might play a role in synchronizing the slow oscillation. Indeed, the particular effectiveness of electrical synapses at transmitting low-frequency events (Landisman et al., 2002; Long et al., 2004) makes them ideally suited to this role. A similar scenario might also exist for TC neurons (Hughes et al., 2004), where electrical synapses are also present (Hughes et al., 2002b), raising the prospect that a certain degree of slow (<1 Hz) wave synchronization can occur locally in the thalamus.

References

Amzica F, Nunez A, Steriade M (1992) Delta frequency (1–4 Hz) oscillations of perigeniculate thalamic neurons and their modulation by light. Neuroscience 51:285–294.

Bal T, McCormick DA (1993) Mechanisms of oscillatory activity in guinea-pig nucleus reticularis thalami in vitro: a mammalian pacemaker. J Physiol (Lond) 468:669–691.

Beurrier C, Congar P, Bioulac B, Hammond C (1999) Subthalamic nucleus neurons switch from single-spike activity to burst-firing mode. J Neurosci 19:599–609.

Bhattacharjee A, Kaczmarek LK (2005) For K^+ channels, Na^+ is the new Ca^{2+}. Trends Neurosci 28:422–428.

BoSmith RE, Briggs I, Sturgess NC (1993) Inhibitory actions of ZENECA ZD7288 on whole-cell hyperpolarization activated inward current (If) in guinea-pig dissociated sinoatrial node cells. Br J Pharmacol 110:343–349.

Broberger C, McCormick DA (2005) Excitatory effects of thyrotropin-releasing hormone in the thalamus. J Neurosci 25:1664–1673.

Brunton J, Charpak S (1997) Heterogeneity of cell firing properties and opioid sensitivity in the thalamic reticular nucleus. Neuroscience 78:303–307.

Contreras D, Steriade M (1995) Cellular basis of EEG slow rhythms: a study of dynamic corticothalamic relationships. J Neurosci 15:604–622.

Contreras D, Curro Dossi R, Steriade M (1993) Electrophysiological properties of cat reticular thalamic neurones *in vivo*. J Physiol (Lond) 470:273–294.

Cox CL, Sherman SM (1999) Glutamate inhibits thalamic reticular neurons. J Neurosci 19:6694–6699.

Crunelli V, Lightowler S, Pollard CE (1989) A T-type Ca^{2+} current underlies low-threshold Ca^{2+} potentials in cells of the cat and rat lateral geniculate nucleus. J Physiol (Lond) 413:543–561.

Crunelli V, Blethyn KL, Cope DW, Hughes SW, Parri HR, Turner JP, Tóth TI, Williams SR (2002) Novel neuronal and astrocytic mechanisms in thalamocortical loop dynamics. Philos Trans R Soc Lond B Biol Sci 357:1675–1693.

Crunelli V, Tóth TI, Cope DW, Blethyn K, Hughes SW (2005) The "window" T-type calcium current in brain dynamics of different behavioural states. J Physiol (Lond) 562:121–129.

Dale N (1993) A large, sustained Na^+- and voltage-dependent K^+ current in spinal neurons of the frog embryo. J Physiol (Lond) 462:349–372.

Destexhe A, Contreras D, Sejnowski TJ, Steriade M (1994) A model of spindle rhythmicity in the isolated thalamic reticular nucleus. J Neurophysiol 72:803–818.

Domich L, Oakson G, Steriade M (1986) Thalamic burst patterns in the naturally sleeping cat: a comparison between cortically projecting and reticularis neurones. J Physiol (Lond) 379:429–449.

Fuentealba P, Crochet S, Timofeev I, Bazhenov M, Sejnowski TJ, Steriade M (2004) Experimental evidence and modeling studies support a synchronizing role for electrical coupling in the cat thalamic reticular neurons *in vivo*. Eur J Neurosci 20:111–119.

Fuentealba P, Timofeev I, Bazhenov M, Sejnowski TJ, Steriade M (2005) Membrane bistability in thalamic reticular neurons during spindle oscillations. J Neurophysiol 93:294–304.

Hodgkin AL, Huxley AF (1952) A quantitative description of membrane current and its application to conduction and excitation in nerve. J Physiol (Lond) 117:500–544.

Hughes SW, Cope DW, Crunelli V (1998) Dynamic clamp study of I_h modulation of burst firing and delta oscillations in thalamocortical neurons *in vitro*. Neuroscience 87:541–550.

Hughes SW, Cope DW, Tóth TI, Williams SR, Crunelli V (1999) All thalamocortical neurones possess a T-type Ca^{2+} "window" current that enables the expression of bistability-mediated activities. J Physiol (Lond) 517:805–815.

Hughes SW, Cope DW, Blethyn KL, Crunelli V (2002a) Cellular mechanisms of the slow (<1 Hz) oscillation in thalamocortical neurons *in vitro*. Neuron 33:947–958.

Hughes SW, Blethyn KL, Cope DW, Crunelli V (2002b) Properties and origin of spikelets in thalamocortical neurones *in vitro*. Neuroscience 110:395–401.

Hughes SW, Lorincz M, Cope DW, Blethyn KL, Kekesi KA, Parri HR, Juhasz G, Crunelli V (2004) Synchronized oscillations at alpha and theta frequencies in the lateral geniculate nucleus. Neuron 42:253–268.

Huguenard JR, Prince DA (1991) Slow inactivation of a TEA-sensitive K current in acutely isolated rat thalamic relay neurons. J Neurophysiol 66:1316–1328.

Huguenard JR, Prince DA (1992) A novel T-type current underlies prolonged Ca^{2+}-dependent burst firing in GABAergic neurons of rat thalamic reticular nucleus. J Neurosci 12:3804–3817.

Hutcheon B, Miura RM, Yarom Y, Puil E (1994) Low-threshold calcium current and resonance in thalamic neurons: a model of frequency preference. J Neurophysiol 71:583–594.

Kim U, McCormick DA (1998) Functional and ionic properties of a slow afterhyperpolarization in ferret perigeniculate neurons *in vitro*. J Neurophysiol 80:1222–1235.

Klockner U, Lee JH, Cribbs LL, Daud A, Hescheler J, Pereverzev A, Perez-Reyes E, Schneider T (1999) Comparison of the Ca^{2+} currents induced by expression of three cloned α1 subunits, α1G, α1H and α1I, of low-voltage-activated T-type Ca^{2+} channels. Eur J Neurosci 11:4171–4178.

Landisman CE, Long MA, Beierlein M, Deans MR, Paul DL, Connors BW (2002) Electrical synapses in the thalamic reticular nucleus. J Neurosci 22:1002–1009.

Lee KH, McCormick DA (1997) Modulation of spindle oscillations by acetylcholine, cholecystokinin, and 1*S*,3*R*-ACPD in the ferret lateral geniculate and perigeniculate nuclei *in vitro*. Neuroscience 77:335–350.

Long MA, Landisman CE, Connors BW (2004) Small clusters of electrically coupled neurons generate synchronous rhythms in the thalamic reticular nucleus. J Neurosci 24:341–349.

McCormick DA, Pape HC (1990) Properties of a hyperpolarization-activated cation current and its role in rhythmic oscillation in thalamic relay neurones. J Physiol (Lond) 431:291–318.

McCormick DA, Huguenard JR, Bal T, Pape HC (1997) Electrophysiological and pharmacological properties of thalamic GABAergic neurons. In: Thalamus (Steriade M, Jones EG, McCormick DA, eds), pp 155–212. Amsterdam: Elsevier.

Monteggia LM, Eisch AJ, Tang MD, Kaczmarek LK, Nestler EJ (2000) Cloning and localization of the hyperpolarization-activated cyclic nucleotide-gated channel family in rat brain. Brain Res Mol Brain Res 81:129–139.

Notomi T, Shigemoto R (2004) Immunohistochemical localization of I_h channel subunits, HCN1–4, in the rat brain. J Comp Neurol 471:241–276.

Perez-Reyes E (2003) Molecular physiology of low-voltage-activated t-type calcium channels. Physiol Rev 83:117–161.

Sanchez-Vives MV, McCormick DA (2000) Cellular and network mechanisms of rhythmic recurrent activity in neocortex. Nat Neurosci 3:1027–1034.

Simon NR, Manshanden I, Lopes da Silva FH (2000) A MEG study of sleep. Brain Res 860:64–76.

Simon NR, Kemp B, Manshanden I, Lopes da Silva FH (2003) Whole-head measures of sleep from MEG signals and the ubiquitous "slow oscillation." Sleep Res Online 5:105–113.

Steriade M, Domich L, Oakson G (1986) Reticularis thalami neurons revisited: activity changes during shifts in states of vigilance. J Neurosci 6:68–81.

Steriade M, Nunez A, Amzica F (1993a) A novel slow (<1 Hz) oscillation of neocortical neurons *in vivo*: depolarizing and hyperpolarizing components. J Neurosci 13:3252–3265.

Steriade M, Nunez A, Amzica F (1993b) Intracellular analysis of relations between the slow (<1 Hz) neocortical oscillation and other sleep rhythms of the electroencephalogram. J Neurosci 13:3266–3283.

Steriade M, Contreras D, Curro Dossi R, Nunez A (1993c) The slow (<1 Hz) oscillation in reticular thalamic and thalamocortical neurons: scenario of sleep rhythm generation in interacting thalamic and neocortical networks. J Neurosci 13:3284–3299.

Steriade M, Contreras D, Amzica F, Timofeev I (1996) Synchronization of fast (30–40 Hz) spontaneous oscillations in intrathalamic and thalamocortical networks. J Neurosci 16:2788–2808.

Steriade M, Timofeev I, Grenier F (2001) Natural waking and sleep states: a view from inside neocortical neurons. J Neurophysiol 85:1969–1985.

Talley EM, Cribbs LL, Lee JH, Daud A, Perez-Reyes E, Bayliss DA (1999) Differential distribution of three members of a gene family encoding low voltage-activated (T-type) calcium channels. J Neurosci 19:1895–1911.

Tennigkeit F, Schwarz DW, Puil E (1998) Modulation of bursts and high-threshold calcium spikes in neurons of rat auditory thalamus. Neuroscience 83:1063–1073.

Timofeev I, Steriade M (1996) Low-frequency rhythms in the thalamus of intact-cortex and decorticated cats. J Neurophysiol 76:4152–4168.

Tóth TI, Crunelli V (2001) Estimation of the activation and kinetic properties of $I_{(Na)}$ and $I_{(K)}$ from the time course of the action potential. J Neurosci Methods 111:111–126.

Tóth TI, Hughes SW, Crunelli V (1998) Analysis and biophysical interpretation of bistable behaviour in thalamocortical neurons. Neuroscience 87:519–523.

Uhlrich DJ, Cucchiaro JB, Humphrey AL, Sherman SM (1991) Morphology and axonal projection patterns of individual neurons in the cat perigeniculate nucleus. J Neurophysiol 65:1528–1541.

Williams SR, Toth TI, Turner JP, Hughes SW, Crunelli V (1997) The 'window' component of the low threshold Ca^{2+} current produces input signal amplification and bistability in cat and rat thalamocortical neurones. J Physiol (Lond) 505:689–705.

Zhang L, Jones EG (2004) Corticothalamic inhibition in the thalamic reticular nucleus. J Neurophysiol 91:759–766.